A gravity current model of cooling mantle plume heads with temperature-dependent buoyancy and viscosity

David Bercovici

Department of Geology and Geophysics, School of Ocean and Earth Science and Technology
University of Hawaii at Manoa, Honolulu

Jian Lin

Department of Geology and Geophysics, Woods Hole Oceanographic Institution
Woods Hole, Massachusetts

Abstract. Gravity currents are a ubiquitous fluid dynamical phenomenon which involve the horizontal spreading of fluid masses under their own weight or buoyancy. A theoretical model is developed to account for the effects of bulk cooling on the dynamics and morphology of geological gravity currents, with particular focus on mantle plume heads spreading beneath the lithosphere. As many geological gravity currents (e.g., plume heads and lava flows) spread, they cool and thereby become more viscous and dense. All gravity currents initially spread at the same rate as the isothermal currents predicted by *Huppert* [1982]. However, currents with temperature-dependent viscosity and/or buoyancy eventually go to a much slower spreading rate than the isothermal currents. Moreover, unlike the isothermal gravity currents, cooling variable-viscosity and/or variable-buoyancy currents do not conserve shape as they spread. Both constant volume and constant volume flux currents with strongly temperature dependent viscosity develop steep-sided flat-topped, plateau shapes which become more rounded once the currents lose most of their heat. Currents with temperature-dependent buoyancy develop inflections or even extensive swelling at their flow fronts. The surface expression of the edge-steepening effect in mantle plume heads is likely to be filtered by lithospheric flexure but may contribute to the flattened plateau shape inferred by *Wessel* [1993] for the Hawaiian swell. The frontal inflation effect due to variable buoyancy may contribute to the dual-lobe structure of the Hawaiian swell gravity anomaly and suggests an alternate physical mechanism for forming the torus- or horseshoe-shaped geochemical patterns in the Galápagos and the Marquesas hotspots. Perhaps most significantly, the gravity current model also predicts the thermal (i.e., degree-of-melting) pattern for Galápagos and Marquesas hotspots more readily than the traditional entrainment models.

Introduction

Many hotspot structures are often thought to result from processes occurring to mantle plumes or plume heads in the deep mantle. Individual volcanic islands on hotspot tracks are typically attributed to a tilt instability in plumes being sheared by plate motion [*Skilbeck and Whitehead*, 1978; *Olson and Singer*, 1985] or to solitary waves propagating along the plume stem [*Olson and Christensen*, 1986; *Scott et al.*, 1986; *Schubert et al.*, 1989; *Helfrich and Whitehead*, 1990]. Geochemical and petrological patterns, such as ring or horeshoe shapes [*Duncan et al.*, 1986; *Geist et al.*, 1988; *Woodhead*, 1992;

White et al., 1993], are interpreted to arise from entrainment of ambient mantle into plumes [*Richards and Griffiths*, 1989; *Griffiths and Campbell*, 1991a] and/or the development of torus-shaped plume heads [*Griffiths*, 1986]. However, the interaction of mantle plumes and plume heads with lithosphere also plays an important role in the evolution and structure of hotspots. For example, sublithospheric lateral spreading of plume heads can lead to secondary flow patterns [*Griffiths and Campbell*, 1991b; *Bercovici*, 1992]. Lithospheric flexure itself may influence volcano spacing [*Vogt*, 1974; *ten Brink*, 1991] and geochemical patterns [*Feighner and Richards*, 1994]. Chemical or physical interaction of plume-induced melting with lithosphere also yields a strong influence on hotspot structure [e.g., *Olson*, 1994; *Phipps Morgan et al.*, 1995].

Clearly, one of the primary means of interaction between plume heads or continuously fed plume tops

(which we hereafter also refer to as plume heads) and overlying lithosphere is through cooling of the plume material. Cooling affects the plume head's buoyant up-lift, spreading rate, melt production, and heating of the overlying lithosphere. Although plumes and plume heads may not undergo extensive cooling during ascent through the mantle [Loper and Stacey, 1983; Griffiths and Campbell, 1990], they are likely to lose significant heat when they come into contact with the lithosphere (especially oceanic), which maintains a large conductive heat flux toward the surface because of its steep verti-cal thermal gradient. Evidence for cooling of plumes is also suggested by petrological and geochemical studies of the Galápagos hotspot [White et al., 1993]. In this study we propose a relatively simple gravity current the-ory for sublithospherically spreading plume heads which is designed to account for the two first-order effects of cooling on plume heads: an increase in viscosity and a loss of buoyancy. Although two-dimensional (2-D) and three-dimensional (3-D) simulations of thermal convec-tion can be used to examine plumes, there are several advantages to obtaining a simple one-dimensional (1-D) theory to describe plume heads. First, it allows us to fo-cus on the dynamics of isolated plume heads with much higher detail and resolution than is possible (econom-ically) with 2-D or 3-D convection models that must necessarily account for the entire convecting layer. A 1-D theory is much easier to solve so that simple ana-lytical and empirical relations for plume head shape and evolution can be obtained. A gravity current model is also readily joined to a lithospheric flexure or melt per-colation model; i.e., a lithospheric or magma dynamics problem is more easily solved if it is coupled only to a simple 1-D theory, as opposed to a 2-D or 3-D convec-tion model.

The relevance of gravity current theory (see the clas-sic work by Huppert [1982]; see also Lister and Kerr, [1989]) to geological problems is potentially endless, its most extensive application being to lava flows [Crisp and Baloga, 1990; Huppert et al., 1982; Fink and Grif-fiths, 1990, 1992; Griffiths and Fink, 1993; Stasiuk et al., 1993]. The application of gravity current theory to mantle plume heads, however, has been more contro-versial. Olson [1990] proposed a gravity current model for the spreading of mantle plume heads beneath the lithosphere. This model was used to demonstrate that a plume head, spreading under its own buoyancy as well as being drawn out by plate motion, could gener-ate a more viable hotspot-swell relief than thermal re-juvenation. However, a potential weakness of this the-ory was pointed out by Griffiths and Campbell [1991b], who showed that the spreading rate of plume heads sur-rounded by a more viscous mantle is controlled by the viscosity of the surrounding mantle, not by the plume viscosity, as assumed in the gravity current theory [see also Koch and Koch, 1995]. Although Olson's model was found by Ribe and Christensen [1994] to be valid

in numerical models of thermal plumes, their study was itself only for a factor of 30 viscosity contrast between the mantle and plume.

The applicability of gravity current theory to plume heads has been most recently advocated by Phipps Mor-gan et al. [1995], who considered the material proper-ties of plume heads as they reach the base of the litho-sphere and undergo partial melting. The melted compo-nent is presumed to percolate into the overlying litho-sphere, while the larger remaining portion of the plume head is depleted in volatiles and consequently has higher viscosity than before melting. This volatile-depleted plume head is likely to have higher viscosity than sur-rounding asthenosphere, thereby satisfying the criterion for gravity current flow, in which the current's flow is controlled by its own viscosity. Moreover, the Phipps Morgan et al. [1995] hypothesis predicts an appropri-ately low geoid-to-topography ratio for the Hawaiian swell, which few models achieve [see Sleep, 1990; Olson, 1990; Ribe and Christensen, 1994]. The low geoid-to-topography ratio occurs because buoyant melt injected into the lithosphere effectively causes rejuvenation, and the higher-viscosity buoyant plume head induces more lithospheric thinning than was previously assumed and thus resides at shallower depths.

Cooling in geological gravity currents has been con-sidered previously, mostly in the context of lava flows. In lava flows, crust formation possibly keeps the flow in-teriors nearly isothermal and hence isoviscous except for a strong skin [Crisp and Baloga, 1990; Fink and Grif-fiths, 1990, 1992; Griffiths and Fink, 1993]. This no-tion, however, was challenged by Stasiuk et al. [1993], who contend that crust formation for many actual lava flows is negligible and that bulk cooling is the dominant thermodynamic effect. Fundamental gravity current theories which account for bulk cooling, as appropri-ate for mantle plumes and possibly lava flows, are rare. Although Phipps Morgan et al. [1995] included ther-mal buoyancy in the total plume head density anomaly, cooling was not considered. The influence of cooling was considered by Stasiuk et al. [1993], who presented empirical scaling laws for bulk viscosity and spreading rate in the presence of heat loss, and Sakimoto and Zu-ber [1995], who examined the influence of cooling on viscosity by prescribing viscosity to decrease uniformly as t^n, where t is time and n is an arbitrary constant. A theoretical model using more self-consistent thermo-dynamics for the cooling of gravity currents with vari-able viscosity was introduced by Bercovici [1994]. This model demonstrated that thermoviscous effects can in-duce significant variations in the evolution and shape of gravity currents. However, this theory did not account for the loss of thermal buoyancy, which is likely to be a significant effect in mantle plume heads. In this paper we expand on this latter theory by including the effects of thermal buoyancy.

Theory

In this section we present the derivation of the general gravity current theory from the basic equations of motion and energy. The final nondimensional equations governing the evolution of the gravity current's thickness and temperature are given by equations (18)–(20).

Flow Law

As with all axisymmetric gravity current theories [see *Huppert*, 1982; *Lister and Kerr*, 1989], radial motion is modeled with the equations for creeping flow of incompressible (or Boussinesq) fluid in a thin cylindrical (i.e., disklike) channel in which horizontal variations in stress and velocity are negligible compared to vertical variations:

$$0 = -\frac{\partial P}{\partial r} + \frac{\partial}{\partial z}\left(\mu \frac{\partial v_r}{\partial z}\right) \tag{1}$$

where r is radius, z is height, P is pressure, v_r is radial velocity, and μ is dynamic viscosity. Viscosity is temperature dependent and described by a simplified rheological law [*Bercovici*, 1992, 1994],

$$\mu(\theta) = \frac{\mu_h \mu_c}{\mu_h + \Delta\mu\theta} \tag{2}$$

where μ_h and μ_c are the viscosities of the fluid at the hottest and coldest temperatures, respectively (thus $\mu_c \geq \mu_h$), $\Delta\mu = \mu_c - \mu_h$, and θ is the dimensionless temperature of the current (see Table 1). This inverse dependence of viscosity on temperature facilitates an analytic derivation of the theory, yet still captures the essential physics of viscous fluid behavior, i.e., that thermal fluctuations cause the largest viscosity anomalies when the fluid is at its coldest.

To derive a nonisothermal gravity current theory in the simplest possible manner, we assume that $0 < \theta \leq 1$ within the current and $\theta = 0$ at its horizontal boundaries. In using isothermal boundaries we essentially assume the gravity current is bounded by a medium with infinite thermal conductivity; in fact, the surrounding medium (especially in the case of mantle plumes) may differ little in conductivity from the current. The partially insulating effect of the outer medium may be offset somewhat in the mantle environment, because a plume head spreads beneath the lithosphere, which, with its steep thermal gradient, conducts heat to the surface relatively rapidly. The horizontal boundaries are at $z = 0$ and $z = -H$, where the lower boundary is deformable (thus $H = H(r,t)$). For application to mantle plumes we describe the current as spreading beneath a solid boundary under its own buoyancy. However, the gravity current theory presented here is still applicable to surface flows when buoyancy is constant. Given that $\theta = 0$ at the top and bottom boundaries, we assume a parabolic temperature profile as a first-order approximation:

Table 1. Control Parameters for the Dimensional Governing Equations (6), (9), and (15)

Parameter	Definition
g *	gravitational acceleration
ρ_1	density of the gravity current at its coldest
ρ_2	density of the medium underlying the current
α	thermal expansivity of the current
κ *	thermal diffusivity of the current
ΔT	temperature drop between the hottest and coldest parts of the current (at time $t = 0$)
$\Delta\rho_C$ *	$\rho_2 - \rho_1$
$\Delta\rho_T$ *	$\rho_1\alpha\Delta T$
$\Delta\rho$	$\Delta\rho_C + \Delta\rho_T$
μ_c *	dynamic viscosity of the current at its coldest
μ_h *	dynamic viscosity of the current at its hottest
$\Delta\mu$	$\mu_c - \mu_h$
$\delta\mu$ *	$3\Delta\mu/5$ if no-slip boundary at $z = -H$ $9\Delta\mu/10$ if free-slip boundary at $z = -H$
C *	12 if no-slip boundary at $z = -H$ 3 if free-slip boundary at $z = -H$
Q *	net volumetric flux into the current supplied by an external fluid source
a *	Gaussian half width of the fluid source
V_o *	initial volume of the current
r_o *	initial radius of the edge of the current

*Explicitly appears in the governing equations and/or the boundary and/or initial conditions.

$$\theta(r,z,t) = -6\Theta(r,t)\frac{z}{H}\left(1 + \frac{z}{H}\right) \tag{3}$$

where Θ is the vertical average of θ. Higher-order (i.e., smaller-scale) contributions to the vertical temperature profile may be important; however, the parabolic contribution must always be the dominant term, and the higher-order contributions typically decay away relatively rapidly because of their large thermal gradients (see Appendix A). Nonetheless, our assumptions about isothermal boundaries and the parabolic temperature profile invariably lead to an overestimate of the cooling of the gravity current (since the surrounding medium is assumed to provide no insulation and the higher-order contributions to the temperature profile are assumed to decay away instantaneously). Therefore a test of these and other, more traditional, gravity current assumptions (see below) requires comparison with experiments.

Density of the gravity current is given by

$$\rho = \begin{cases} \rho_1(1 - \alpha\Delta T\theta) & -H \leq z \leq 0 \\ \rho_2 & z < -H \end{cases} \tag{4}$$

where ρ_1 is the maximum density of fluid in the gravity current (i.e., the density of the coldest fluid), ρ_2 is the density of the underlying medium (and $\rho_2 \geq \rho_1$), α is

thermal expansivity, and ΔT is the maximum temperature difference between the hottest and coldest parts of the current (at time $t = 0$). Assuming the current is approximately vertically hydrostatic (i.e., vertical viscous forces are negligible), then $\partial P/\partial z = -\rho g$ [see Huppert, 1982], leading to

$$P = \Delta\rho_C gH + \Delta\rho_T gH\Theta\left(1 - 3\frac{z^2}{H^2} - 2\frac{z^3}{H^3}\right)$$
$$+P(-z_o) - \rho_2 g z_o - \rho_1 g z \qquad (5)$$

where $\Delta\rho_C = \rho_2 - \rho_1$ is the chemical density contrast between the gravity current and the underlying medium, $\Delta\rho_T = \rho_1\alpha\Delta T$ is the thermal density contrast within the current, and z_o is some reference depth beneath the current (i.e., $z_o > H$). Substituting (5) and (2) into (1) and integrating 3 times over depth yields (see Appendix B) the volumetric flux per unit length,

$$q = \int_{-H}^{0} v_r dz = -\frac{gH^2}{2C\mu_h\mu_c}(\mu_h + \delta\mu\Theta)$$
$$\times \frac{\partial}{\partial r}(\Delta\rho_C H^2 + \Delta\rho_T H^2\Theta) \qquad (6)$$

where

$$\left(C, \frac{\delta\mu}{\Delta\mu}\right) = \left(12, \frac{3}{5}\right) \qquad (7)$$

if the lower boundary (at $z = -H$) is no-slip (i.e., $v_r = 0$) and

$$\left(C, \frac{\delta\mu}{\Delta\mu}\right) = \left(3, \frac{9}{10}\right) \qquad (8)$$

if the lower boundary is free-slip (i.e., $\partial v_r/\partial z = 0$). The contribution from the chemical buoyancy in (6) is derived exactly, whereas the influence of thermal buoyancy is simplified slightly (see Appendix B).

Information about the radial velocity boundary conditions on the deformable surface is contained within the constants C and $\delta\mu$. A free-slip boundary at $z = -H$ is appropriate for surface gravity currents (e.g., lava flows) or if the viscosity of fluid adjacent to the free surface is less than or not greatly different from the current's viscosity [Huppert, 1982]. This condition is therefore also appropriate for plume heads as described by Phipps Morgan et al. [1995].

We include discussion of a no-slip condition at $z = -H$ to show that it does not lead to a set of equations significantly different from the more widely accepted free-slip condition. A no-slip boundary at $z = -H$ is only partially appropriate for plume heads spreading into a higher-viscosity medium; i.e., it gives an incomplete description of all the forces on such a plume head. Although it approximates the drag of the high-viscosity medium on the horizontal free surface of the gravity current, it does not account for the normal stresses on the edge of the gravity current as it propagates into the outer medium. These normal stresses are important for controlling the spread of gravity currents, as noted by Griffiths and Campbell [1991]. The normal stresses are somewhat approximated in the present theory by the presence of a cold, high-viscosity plug at the edge of the gravity current. However, this effect is only a proxy for the true physics, assuming the high-viscosity plug has a viscosity comparable to that of the outer medium; even so, the plug effect is only significant after cooling becomes substantial and is therefore not present in the plume head's early evolution.

The use of channel flow theory in (1) and the hydrostatic approximation leading to (5) are valid as long as horizontal variations in H are much greater than H itself. This "long-wavelength" or "small-slope" approximation is violated by all gravity current theories near the edge of the current [Huppert, 1982]. Given this and our assumptions about the vertical temperature profile, experimental verification is desirable. Basic gravity current theories predict experimental gravity currents remarkably well [e.g., Huppert, 1982; Didden and Maxworthy, 1982]. In this paper we will also compare, to the extent possible, the features of our theoretical gravity currents to experimental ones, in particular the laboratory gravity currents of Stasiuk et al. [1993].

Continuity

The rate of change of the thickness of the gravity current is prescribed by conservation of mass; i.e.,

$$\frac{\partial H}{\partial t} = -\frac{1}{r}\frac{\partial}{\partial r}(rq) + W(r) \qquad (9)$$

where W is the vertical velocity of material being injected into the current through one of the horizontal boundaries. The fluid source is explicitly prescribed by W because the form of q in (6) precludes a tractable flux boundary condition (unless $\Delta\rho_T = 0$; see Bercovici [1994]). The net volumetric flux into the current is

$$Q = 2\pi\int_0^\infty Wr\,dr \qquad (10)$$

which we assume is constant. For simplicity, we define W to be a Gaussian function of r with half width a and thus

$$W = \frac{Q}{\pi a^2}e^{-r^2/a^2}. \qquad (11)$$

Integrating (9) over area, we obtain the net volume of the gravity current,

$$2\pi\int_0^\infty Hr\,dr = Qt + V_o \qquad (12)$$

where V_o is the initial volume of the current, and we assume that q is finite at $r = 0$ and vanishes at some finite r, where the gravity current ends. In this paper we consider only cases of constant volumetric flux in which $Q > 0$ and $V_o \geq 0$, or constant volume whence $Q = 0$ and $V_o > 0$.

Temperature

Assuming that vertical diffusion through the horizontal boundaries is the primary sink of heat, we employ a simple boundary layer transport law to model the evolution of temperature:

$$\frac{\partial\theta}{\partial t} + \nabla \cdot (\mathbf{v}\theta) = \kappa\frac{\partial^2\theta}{\partial z^2} = -\frac{12\kappa\Theta}{H^2} \tag{13}$$

where κ is thermal diffusivity and $\mathbf{v}$ is the velocity vector. To obtain a 1-D equation for the vertically averaged temperature Θ, we integrate (13) over the volume of a thin cylindrical shell from $z = -H$ to 0 and from r to $r + dr$ where $dr \ll r$. Dividing this integral by $2\pi r\, dr$, taking the limit of $dr \to 0$, and given that $\int_{-H}^{0} v_r\theta\, dz \approx q\Theta$ (see Appendix B), we arrive at a conservative form of the temperature equation

$$\frac{\partial(H\Theta)}{\partial t} + \frac{1}{r}\frac{\partial}{\partial r}(rq\Theta) = W - \frac{12\kappa\Theta}{H}. \tag{14}$$

The first term on the right side of (14) arises from the bulk vertical temperature flux into the top or bottom of the cylindrical shell due to the fluid source, which we assume injects material at the maximum dimensionless temperature of 1. Using the continuity equation (9), we transform (14) into a more traditional advection-diffusion law:

$$\frac{\partial\Theta}{\partial t} + \frac{q}{H}\frac{\partial\Theta}{\partial r} = \frac{W(1-\Theta)}{H} - \frac{12\kappa\Theta}{H^2}. \tag{15}$$

Nondimensionalization

The dimensional governing equations for the gravity current are (6), (9), and (15). We nondimensionalize H by

$$H_o = \begin{cases} [2C\mu_h\mu_c Q/\Delta\rho g(\mu_h + \delta\mu)]^{1/4} & Q > 0 \\ [24C\kappa\mu_h\mu_c V_o/\Delta\rho g(\mu_h + \delta\mu)]^{1/6} & Q = 0 \end{cases}, \tag{16}$$

r and a by

$$R = \sqrt{\frac{\Delta\rho g H_o^5(\mu_h + \delta\mu)}{24C\kappa\mu_h\mu_c}}, \tag{17}$$

flux q by $12\kappa R/H_o$, and time t by $H_o^2/12\kappa$, where $\Delta\rho = \Delta\rho_C + \Delta\rho_T$. The dimensionless governing equations thus become

$$\frac{\partial H}{\partial t} = -\frac{1}{r}\frac{\partial}{\partial r}(rq) + W' \tag{18}$$

$$\frac{\partial\Theta}{\partial t} + \frac{q}{H}\frac{\partial\Theta}{\partial r} = \frac{W'}{H}(1-\Theta) - \frac{\Theta}{H^2} \tag{19}$$

$$q = -\left(\frac{1+\nu\Theta}{1+\nu}\right)H^2\frac{\partial}{\partial r}(fH^2 + (1-f)H^2\Theta), \tag{20}$$

where

$$W' = \frac{Q'}{\pi a^2}e^{-r^2/a^2} \tag{21}$$

Table 2. Control Parameters for the Dimensionless Governing Equations (18)–(20)

Parameter	Definition
f	$\Delta\rho_C/(\Delta\rho_C + \Delta\rho_T)$
ν	$\delta\mu/\mu_h$
Q'	net flux of the fluid source; equals 1 or 0
a	Gaussian half-width of the fluid source
V'	initial volume of the current (see (23))
r_o	initial radius of the edge of the current

in which $Q' = 0$ for constant volume currents, and $Q' = 1$ for constant volumetric flux currents. The two free parameters which control the dependence of buoyancy and viscosity on temperature are

$$f = \frac{\Delta\rho_C}{\Delta\rho_C + \Delta\rho_T}, \qquad \nu = \frac{\delta\mu}{\mu_h}, \tag{22}$$

respectively (see Table 2). Note that the viscosity scale is $\mu_c\mu_h/(\mu_h + \delta\mu)$; this insures that currents which differ only in ν would spread identically if not for cooling (e.g., q is independent of ν in (20) when $\Theta = 1$). Moreover, the most significant information about the velocity boundary conditions (in particular the constant C) has been absorbed into the length, thickness, and time scales.

Boundary and Initial Conditions

Assuming there are no point sources of mass or heat (i.e., $a \neq 0$), then H, Θ, $\partial H/\partial r$, $\partial\Theta/\partial r$, and thus q are finite and continuous at $r = 0$. Given this result, the only relevant boundary condition for (18) is that $rq = 0$ at $r = 0$. This is true for either constant volume or constant volume flux currents.

For constant volume currents ($Q' = 0$), Θ has an a extremum (a minimum or maximum) at $r = 0$ (since $r = 0$ is a symmetry point), and thus the boundary condition for (19) is $\partial\Theta/\partial r = 0$ at $r = 0$. For constant volume flux currents ($Q' = 1$) we assume fluid at the center of the current is at the maximum temperature, and thus $\Theta = 1$ at $r = 0$.

If the gravity current has an initial volume ($V_o > 0$), then the shape of H and Θ at $t = 0$ must be defined. Regardless of shape the gravity current at time $t = 0$ must have dimensionless volume

$$2\pi\int_0^\infty Hr\,dr = V' = \begin{cases} V_o/R^2 H_o & Q' = 1 \\ 1 & Q' = 0 \end{cases} \tag{23}$$

(the volume at a later time is, of course, $2\pi\int_0^\infty Hr\,dr = Q't + V'$). We arbitrarily choose the initial current to have the shape of an isothermal constant volume current [Huppert, 1982], i.e.,

$$H(r, t = 0) = \begin{cases} 4V'\left(1 - r^2/r_o^2\right)^{1/3}/3\pi r_o^2 & r \leq r_o \\ 0 & r > r_o \end{cases} \tag{24}$$

where r_o is the radius of the edge of the initial current. We make the initial temperature Θ nearly uniformly equal to 1 inside the current yet analytically smooth and continuous at the current's edge by using a super-Gaussian function:

$$\Theta(r, t = 0) = e^{-(r/r_o)^{20}} \qquad (25)$$

Results

Equations (18), (19), and (20) are solved numerically with simple upwind finite differences for the temperature transport equation and with finite-volumes [Patankar, 1980] for the continuity equation. To avoid singularities, the equations are spatially transformed to a new independent variable $x = r^2/2$. To the same end the thermal diffusion term $-\Theta/H^2$ is replaced by $-\Theta/\max(H^2, 10^{-4})$. In all solutions we use 501 grid points evenly spaced in x; convergence tests show that the solutions are well resolved with 201 grid points.

We consider only basic classes of gravity currents, i.e., with constant volume and constant volume flux. In each class we examine the separate and combined effects of allowing buoyancy and viscosity to be temperature dependent.

Constant Volume Currents

We begin all the constant volume currents ($Q' = 0$, $V' = 1$) with an inital edge radius of $r_o = 0.1$ and examine the evolution of H, Θ, and the rate of spreading and collapse of the current for $0.01 \leq f \leq 1$ and $0 \leq \nu \leq 10^5$. We do not consider the case with $f = 0$, because it is unreasonable to assume that fluid in a current with $f = 0$ would continue to adhere to the upper rigid boundary (at $z = 0$) when $\Theta = 0$ (i.e., when all of its buoyancy vanishes).

Rather than give an exhaustive survey of all possible numerical solutions we show a few solutions which exhibit the most fundamental tendencies. The evolution of the thickness H and temperature Θ for four basic gravity currents is illustrated in Figure 1. The isoviscous, constant density current (i.e., with $\nu = 0$, $f = 1$) maintains a self-similar shape while it collapses, as predicted by Huppert [1982]. When cooling is allowed to affect buoyancy and/or viscosity the self-similar nature is lost. In all cases with variable buoyancy ($f < 1$) and/or viscosity ($\nu > 0$) the front of the current is much steeper than it is for the isoviscous, constant density case. The steepness of the current's edge clearly compensates for the pluglike effect of the colder material by creating a large pressure gradient. In the cases with $f < 1$ the current's thickness H initially develops an inflection near the edge (i.e., either a flattening or uplifted rim), which is enhanced when viscosity is also variable. The width of the raised rim is dependent on the temperature gradient at the edge of the current; this dependency leads, in some cases, to a sharp rim at the start of the current's collapse since, at that time,

the temperature gradient near the edge is very steep (e.g., Figure 1, bottom). Once the currents lose most of their heat, they assume a smooth, dome shape similar to that of the isothermal current [Huppert, 1982]; this occurs because by this time the currents are essentially isothermal (i.e., $\Theta \approx 0$).

Figure 2 shows the maximum thickness H_{max}, edge radius r_{max}, and maximum temperature Θ_{max} versus time for the same cases shown in Figure 1. For the isothermal gravity current, H_{max} collapses as $t^{-1/4}$ and r_{max} propagates as $t^{1/8}$, as predicted by Huppert [1982]. Up until time $t = 1$ (i.e., one diffusion time) the variable viscosity and/or density currents parallel the isothermal current; i.e., H_{max} and r_{max} have the identical power law dependences on time, even though their shapes may be much different from the shape of the isothermal current. After $t = 1$ the temperature drops rapidly, causing the collapse and spreading of the current to slow significantly. After $t \approx 2$ the H_{max} and r_{max} curves for the variable viscosity and/or density cases have nearly flat slopes; i.e., the gravity currents nearly freeze in place.

The variable viscosity currents with constant density ($f = 1$) appear to maintain a self-similar profile up until time $t = 1$ (i.e., one diffusion time). Since this profile changes at later times, a general similarity solution of the equations of motion is not available. However, these gravity currents for $t < 1$ fit a profile of the form

$$\frac{H}{H_{max}} = \left[1 - \left(\frac{r}{r_{max}} \right)^2 \right]^{1/\gamma} \qquad (26)$$

where $\gamma = 3$ when $\nu = 0$ and $\gamma \to \infty$ as $\nu \to \infty$. The dependence of γ on ν would of course be useful, and similarity arguments can be used to help find this dependence. In particular, since $r_{max} \sim t^{1/8}$ (temporarily), we can expect (as with Huppert's solution) a similarity solution for H of the form

$$H = B(\eta)/t^{1/4} \qquad (27)$$

where $\eta = r/t^{1/8}$, for which (18) combined with (20) becomes (after integrating in η and applying the condition that both B and $dB/d\eta$ are finite at $\eta = 0$)

$$8AB^2\frac{dB}{d\eta} + \eta = 0 \qquad (28)$$

where $A = 2(1 + \nu\Theta)/(1 + \nu)$. For a similarity profile of the form of (26) to satisfy (28) it is necessary that $A \sim B^{b(\nu)}$ in which $\gamma = 3 + b(\nu)$. The function $b(\nu)$ is found through a least squares fit of various numerically obtained profiles (for $0 \leq \nu \leq 10^5$); this search indicates that

$$\gamma = 3 + \log(1 + \nu)^{7/5}; \qquad (29)$$

Figure 3 shows that (26) with this γ provides a very good fit to the numerical solutions over several orders of magnitude change in the viscosity contrast parameter ν.
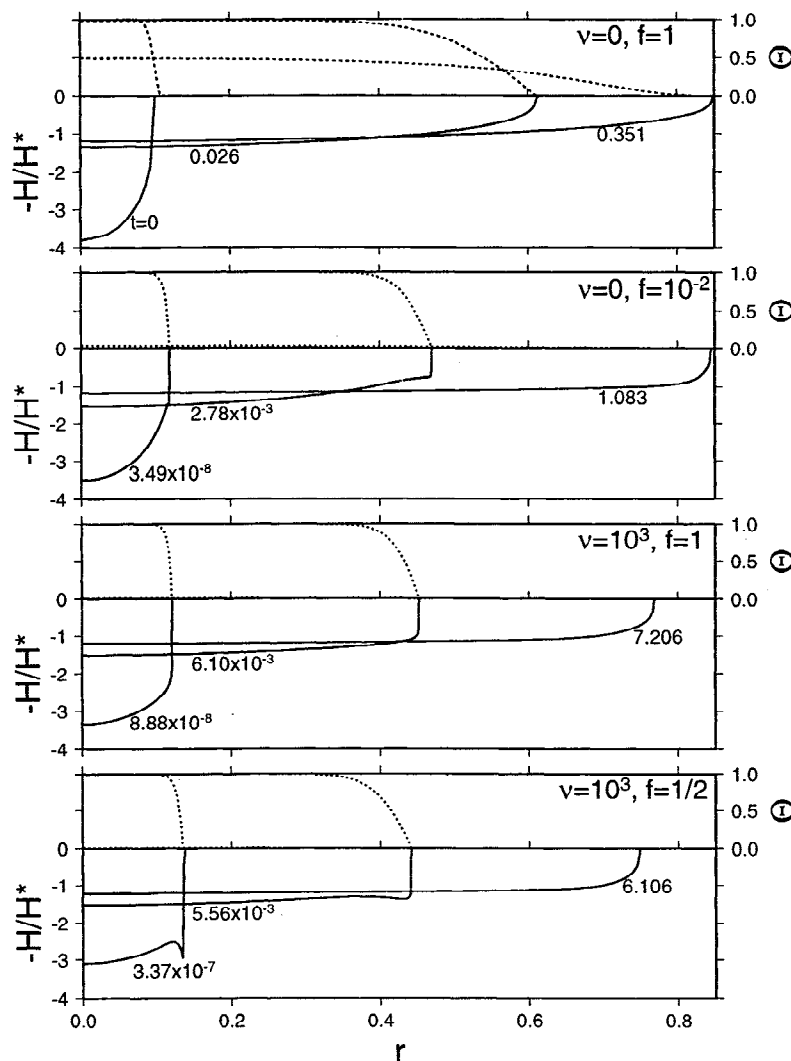
Figure 1. Constant volume gravity current thickness H (solid lines) and temperature Θ (dashed lines) versus radius r at different times and for different values of viscosity contrast ν and chemical buoyancy f. Time t, ν, and f are denoted on the figures. Thickness H is scaled by $H^* = \log(e + H_{max})$ so that the currents are visible after time $t = 0$. All solutions are started with $r_o = 0.1$ (see equations (24) and (25)).

Cases with $f < 1$ have profiles with changes in curvature or even have multiple extrema; these cases also undergo considerable alterations through time even while $t < 1$. Thus there is no simple similarity profile (as yet) with which to model the variable density currents.

Constant Volume Flux Currents

The evolution of four constant flux gravity currents (with the same combinations of ν and f as in Figure 1) is shown in Figure 4; in all cases $Q' = 1$, $V' = 0$ and the source half width is $a = 0.1$. Since these currents are fed by a source with finite width, they do not exactly correspond to the gravity current solutions of Huppert, which are fed by point sources and whose thicknesses are therefore singular at the origin. Even so, the isothermal ($\nu = 0$, $f = 1$) case displays an approximately self-similar shape throughout its evolution. Moreover, the

current's thickness does not change appreciably with time, in basic agreement with Huppert's theory, which predicts that the average thickness is independent of time. In isothermal currents therefore the growth in volume occurs primarily through spreading and very little through thickening.

The isoviscous current with predominantly thermal buoyancy ($\nu = 0$, $f = 10^{-2}$) displays a markedly different evolution: It maintains a very steep front, and much of the volume increase is accommodated by swelling of the flow front. In fact, after one diffusion time ($t = 1$) the maximum height occurs near the current's edge and not at its center. The swell likely arises to compensate for the loss of buoyancy in the colder perimeter of the current.

Chemically buoyant currents ($f = 1$) with variable viscosity develop steep fronts and nearly uniformly thick interiors, much like the constant volume currents. These
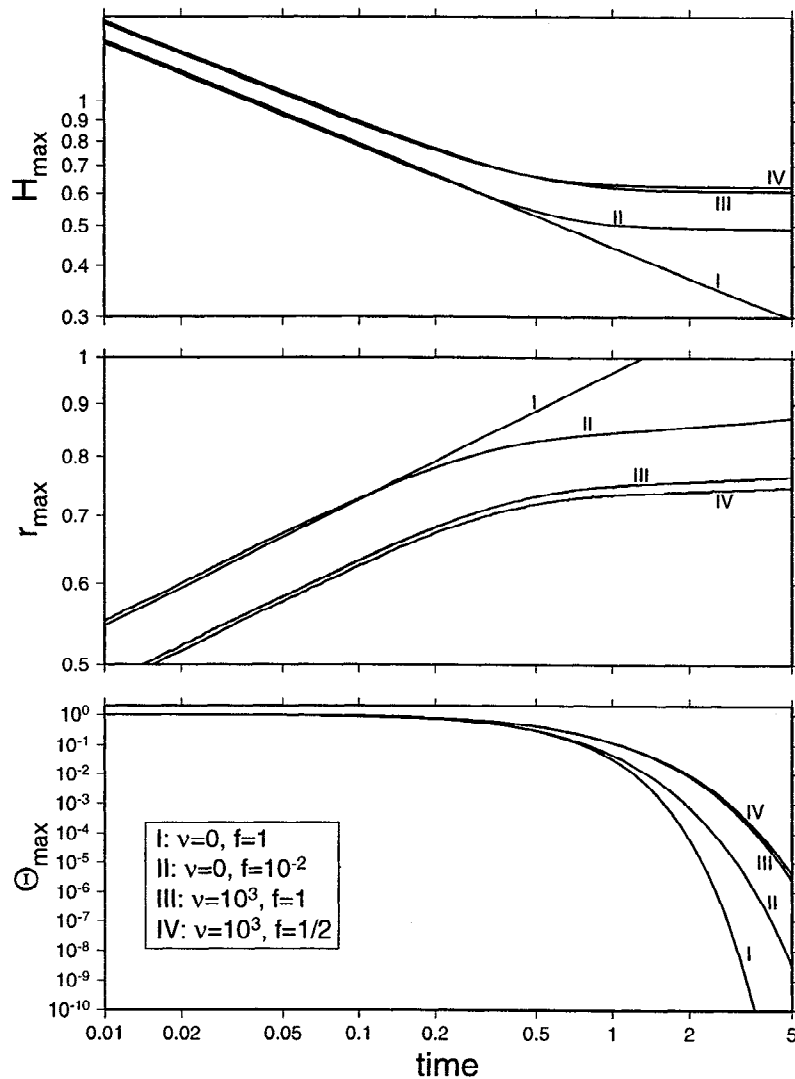
Figure 2. Maximum thickness H_{max}, edge radius r_{max}, and maximum temperature Θ_{max} versus dimensionless time for the cases of Figure 1. All curves are shown on a log-log scale.

currents also grow in volume as much by thickening as spreading. Up until one diffusion time they maintain a nearly self-similar shape; after this time the edge becomes more rounded.

Currents with both variable viscosity and density begin with flat, steep-edged profiles. However, after some time the flow front swells, eventually retaining the maximum thickness. The current's center becomes a region of minimum thickness, in stark contrast to the constant density currents.

The evolution of the gravity current's temperature field is notable. For all the currents, and especially the isoviscous ones, the temperature field essentially reaches an equilibrium, Gaussian-shaped profile with a dimensionless half width of unity. The currents with variable viscosity continue to thicken with time, thereby becoming more self-insulating and thus allowing the temperature profile to propagate very slowly beyond $r = 1$.

Nevertheless, the approach to equilibrium of the temperature field causes a distinct bifurcation in the evolutions of the variable viscosity and/or density gravity currents. It is at this point that the temperature field no longer propagates with the gravity current; the current thus thickens and/or changes shape to be able to push out its cold frontal mass.

The temporal changes in maximum thickness H_{max} and edge radius r_{max} are shown in Figure 5. The thickness of the isothermal current changes only by approximately 30% from $t = 0.1$ to $t = 10$. In contrast, currents with variable viscosity and/or density thicken considerably with time. Most notable is that when the flow front for the variable density currents becomes thicker than the flow center, the H_{max} curve changes slope radically at about $t = 2$; the time for this slope break is apparently independent of f and ν. The break in slope, however, does not affect the spreading rate, as
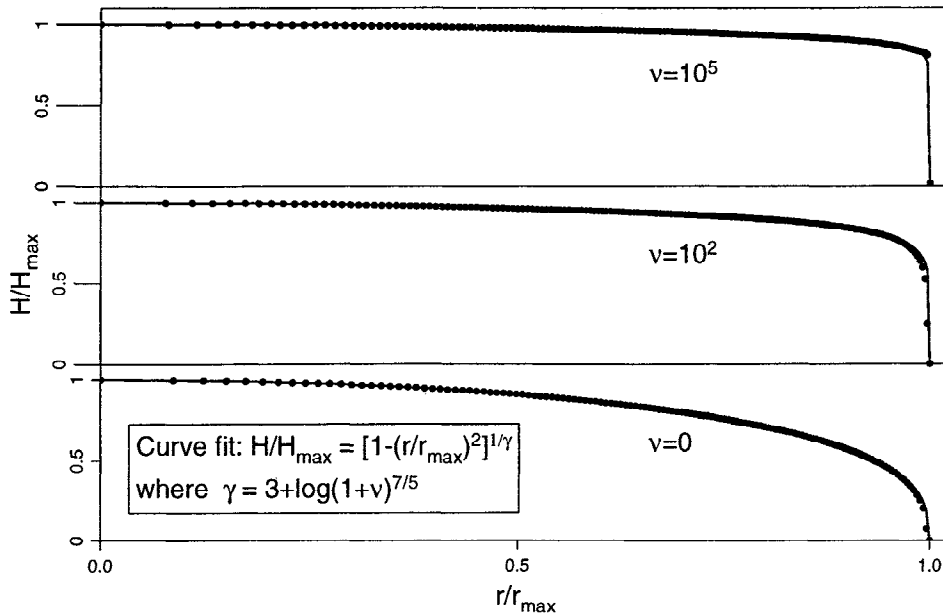
Figure 3. Numerical solutions (solid circles) and approximate self-similar shapes from (26) (solid line) for various constant volume, variable-viscosity gravity currents with $f = 1$. The relation between the shape parameter γ and ν is given in the figure and in equation (29).

manifest in the r_{max} versus t curves. The inclusion of variable viscosity and/or density, however, does cause slower spreading rate as expected.

Like the constant volume currents, the constant flux, constant density, variable viscosity currents display nearly self-similar shapes during times in which the current's edge is sufficiently far from the source and not too far beyond $r = 1$. Once the edge extends beyond $r = 1$, the temperature field stops propagating with the gravity current, causing the current to change shape. A similarity profile was suggested by *Stasiuk et al.* [1993], who investigated constant volume flux, variable viscosity gravity currents with laboratory experiments. Their profile has the form of

$$\frac{H}{H_{max}} = \left[1 - \frac{r}{r_{max}}\right]^{1/\gamma} . \qquad (30)$$

In the limit of an isoviscous current, $\gamma = 3$, corresponding to the approximate solution suggested by *Huppert et al.* [1982]. We can employ this profile to determine (as with the constant volume currents) a useful relation between γ and ν. However, a rigorous fit between the numerical solutions and (30) is more difficult to obtain. The approximate solution of *Huppert et al.* [1982] for the $\nu = 0$ case is only valid near the edge of the current; thus the fit cannot be exact everywhere, and the choice of H_{max} (i.e., H at $r = 0$) in (30) is arbitrary. We choose H_{max} so that the curve defined by (30) matches the numerical solution near the edge, i.e., at $r/r_{max} = 0.9$. We find that for $0 \le \nu \le 10^5$, equation (29) for the constant volume currents is also reasonably applicable for the constant flux currents (Figure

6), though it does not yield quite as good a fit for the intermediate values of ν (i.e., $10 \le \nu \le 100$).

Discussion

Energy and Equilibrium

The relatively sudden changes in inflation rate for the constant volume flux currents with variable viscosity and buoyancy (Figure 5) can be understood by considering states of thermal equilibrium for these currents. The integral of (14) over the total horizontal area is, after nondimensionalizing (see equations (16) and (17)),

$$2\pi \frac{d}{dt} \int_0^\infty H\Theta r dr = 1 - 2\pi \int_0^\infty \frac{\Theta}{H} r dr \qquad (31)$$

which essentially describes the rate of change of net internal energy of the current. Thus, although the volume of a continuously fed current never reaches equilibrium (i.e., it must always grow), its internal energy approaches equilibrium as

$$\int_0^\infty \frac{\Theta}{H} r dr \to \frac{1}{2\pi}. \qquad (32)$$

This disparity of equilibria is at the root of the large transitions in the evolution of these gravity currents. For example, until a constant flux current achieves the thermal equilibrium condition (32), it flows at its hottest with a nearly constant average temperature (i.e., before cooling has become significant). After the equilibrium condition (32) is attained, Θ reaches a
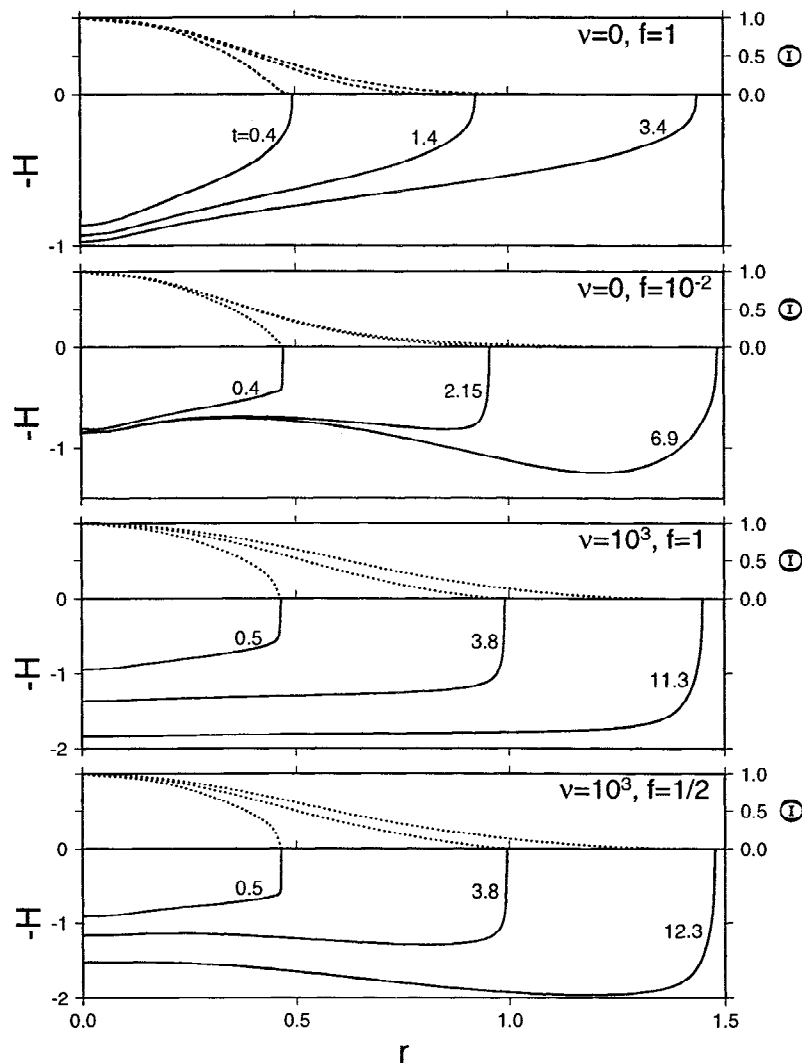
Figure 4. Constant volume flux gravity current thickness H (solid lines) and temperature Θ (dashed lines) versus radius r at different times and for same values of ν and f as in Figure 1. Time t, ν, and f are denoted on the figures. For all solutions the half width of the central fluid source is $a = 0.1$, and there is no inital volume (i.e., $V' = 0$).

steady state, and the temperature distribution no longer spreads with the gravity current; the outer region of the current subsequently spreads at the coldest temperature, with all the attendant changes in buoyancy and viscosity.

Comparison to Laboratory Experiments and Applications to Lava Flows

Stasiuk et al. [1993] presented laboratory experiments for cooling surface gravity currents with temperature-dependent viscosity. In these experiments, room temperature glucose syrup was ejected at a constant rate onto the flat base of a tank filled with a colder aqueous solution. Crust formation was therefore suppressed in these experiments and in this regard they are comparable to our theory.

The most important test of our theory concerns our two main assumptions about loss of heat out of the grav-

ity current. First, we have assumed that the vertical temperature profile adjusts to a parabolic shape rapidly when the gravity current first starts to spread. Second, we assume that the horizontal boundaries are isothermal; this condition is equivalent to having the boundaries in contact with an infinitely conducting medium, whereas in fact the surrounding medium does not have any higher thermal conductivity than the gravity current. Both assumptions therefore lead to excessive heat loss, especially near the beginning of the current's evolution. In this regard, the experiments of Stasiuk et al. are a good test, since the laboratory gravity currents were surrounded by fluid of similar composition (i.e., mainly water) and thermal conductivity (although the effective conductivity of the surrounding fluid was most likely increased by free convection). However, the laboratory currents are continuously supplied, and their density contrast with the surrounding solution was
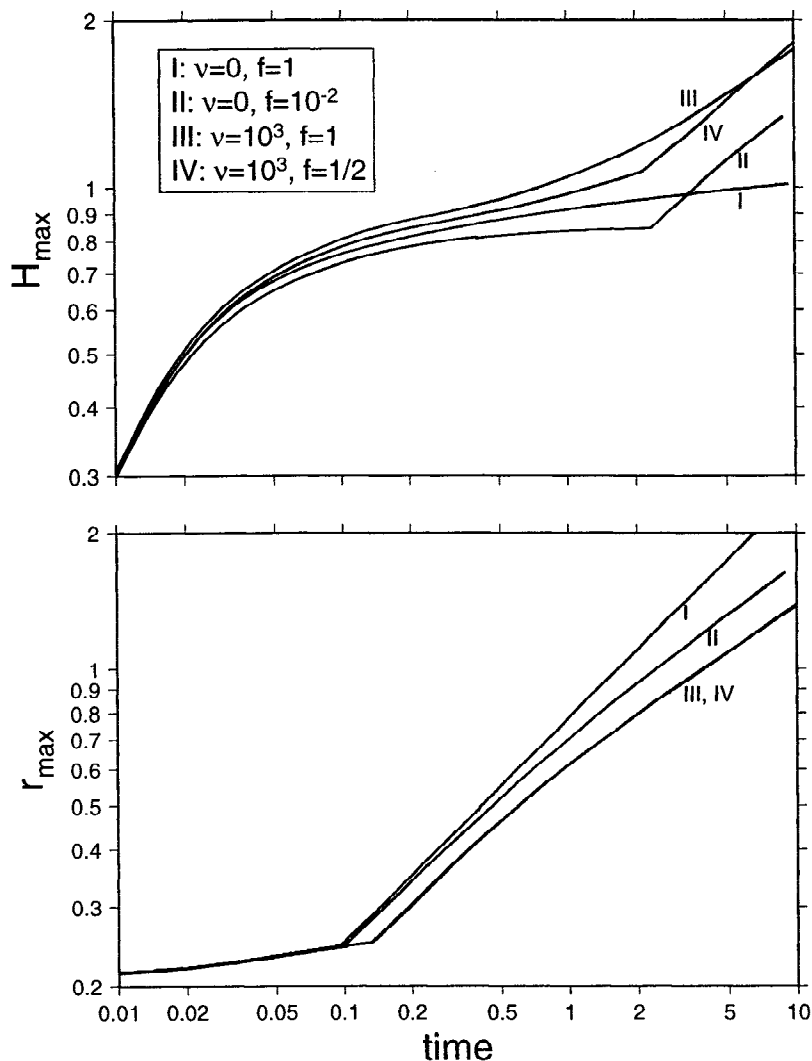
Figure 5. Maximum thickness H_{max} and edge radius r_{max} versus dimensionless time for the cases of Figure 4. All curves are shown on a log-log scale.

much larger than their thermal density anomaly; thus these expreriments are only comparable to our theoretical cases with $f = 1$ and constant volume flux. Moreover, given differences between several features of the theoretical and laboratory models (e.g., viscosity laws and shape of the feeder conduit), a precise quantitative comparison is intractable.

Figure 7a shows profiles of H as a function of r at three different times for one of Stasiuk et al.'s experiments. Early in the experiment the current has a profile similar to that predicted by *Huppert* [1982], though with a slightly steeper front than the fitted curve suggests. This differs from our model prediction, which indicates that a current would develop a steeper edge earlier in its evolution (Figure 4, third frame). This implies that our model indeed overestimates the amount of cooling that occurs near the start of the experiment, as expected. At later times in the experiment, the current develops a steep-sided edge. Moreover, the interior of

the current flattens (i.e., the slope of H near $r = 0$ diminishes through time), and the entire current thickens considerably. All these features (i.e., steepening of the edge, flattening and thickening of the interior) are quite well predicted by our model gravity currents (Figure 4, third frame). The edge-steepening feature provides a particularly important verification; as with all gravity current models, the edge of the current is where the small-wavelength (i.e., channel flow) approximation is most severely violated.

Figure 7b shows data from the above experiment for the spreading rate of the gravity current. A similar plot of our model case with $\nu = 1000, f = 1$ is shown in Figure 7c for comparison. Experiment and theory concur that the spreading rate of the gravity current is initially rapid and similar to that of the isothermal current, but eventually approaches a much slower spreading rate. The diminishing spreading rate is, of course, coincident with the thickening interior. In contrast to the isother-
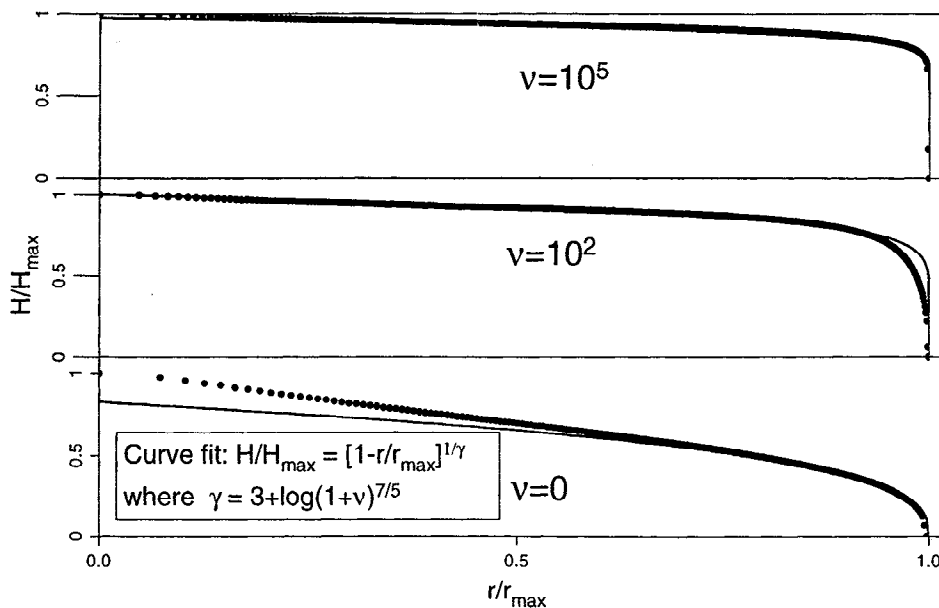
Figure 6. Numerical solutions (solid circles) and approximate self-similar shapes from (30) (solid line) for various constant volume flux, variable-viscosity gravity currents with $f = 1$. The relation between the shape parameter γ and ν is given in equation (29).

mal current, which grows in volume almost exclusively by spreading, the cooling temperature-dependent viscosity currents grow by both thickening and spreading. Therefore, for the gravity currents with $f = 1$, the experiments are modeled well by our theory for most of the time span of the gravity current; some deviation between theory and experiment does occur early in the currents' evolution. Experiments with gravity currents with temperature-dependent buoyancy, as relevant to the theoretical cases with $f < 1$, are not, to our knowledge, available. Although there are experiments with thermal plume heads spreading beneath an impermeable lid [e.g., *Griffiths and Campbell*, 1991b; *Bercovici*, 1992], these plume heads are moving into a more viscous medium, and thus their spreading is controlled by the viscosity of the outer medium. The theory here is most appropriate for gravity currents moving into a medium that is less viscous; for such currents there are no known experiments that also account for loss of buoyancy.

The experiments of Stasiuk et al. differ from those of others who have modeled lava flows [e.g., *Fink and Griffiths*, 1990, 1992; *Griffiths and Fink*, 1993] in that crust formation was essentially suppressed. Stasiuk et al. argue that crust formation is negligible and that bulk cooling is necessarily the dominant effect; insofar as this contention is valid, the gravity current model presented here is reasonably applicable to lava flows. Such gravity current flow may be seen in various volcanological forms, such as mesa lavas and *tortas* (*S. Self*, personal communication, 1994), submarine flat-topped volcanoes on abyssal plains [*Smith and Cann*, 1993; *Smith et al.*, 1995], and steep-sided domes on Venus [*Pavri et al.*, 1992].

Applications to Hotspots and Hotspot Swells

The steep-sided plateau shape of our currents with temperature-dependent viscosity may be manifested in the shape of the Hawaiian swell. Profiles of the swell taken perpendicular to plate motion suggest a flattening near the center, once volcanic loading and associated flexure are essentially removed [see *Wessel*, 1993, Figure 6]. However, given the filtering of short-wavelength effects by lithospheric flexure, the broad morphology of the Hawaiian swell may not be unique enough to distinguish between plume-head models (see also *Olson and Nam* [1986], *Griffiths et al.* [1989], and *Phipps Morgan et al.* [1995]).

However, it is possible that the Hawaiian swell partially reflects the frontal inflation effect seen in our model gravity currents with temperature-dependent buoyancy. The geoid of the Hawaiian swell displays a distinct dual-lobe feature, i.e., two broad geoid highs, one on either side of the volcanic chain [*Wessel*, 1993, Plate 1]. This feature is typically attributed to downward flexure at the center of swell due to the volcanic load. However, the amount of flexure due to the volcanic load is dependent on assumptions about the volcanic mass itself and the lithospheric elastic thickness, neither of which are precisely known [*McNutt and Shure*, 1986]. While such flexure is clearly an important (possibly even dominant) effect, it may be not be the only process causing the dual-lobe structure. It is plausible that the origin of this structure is partially caused by the shape of the plume head itself. If the plume head's edge thickens, as predicted by the gravity current model, it would potentially induce a dual-lobe structure. Although thermal buoyancy in the swollen
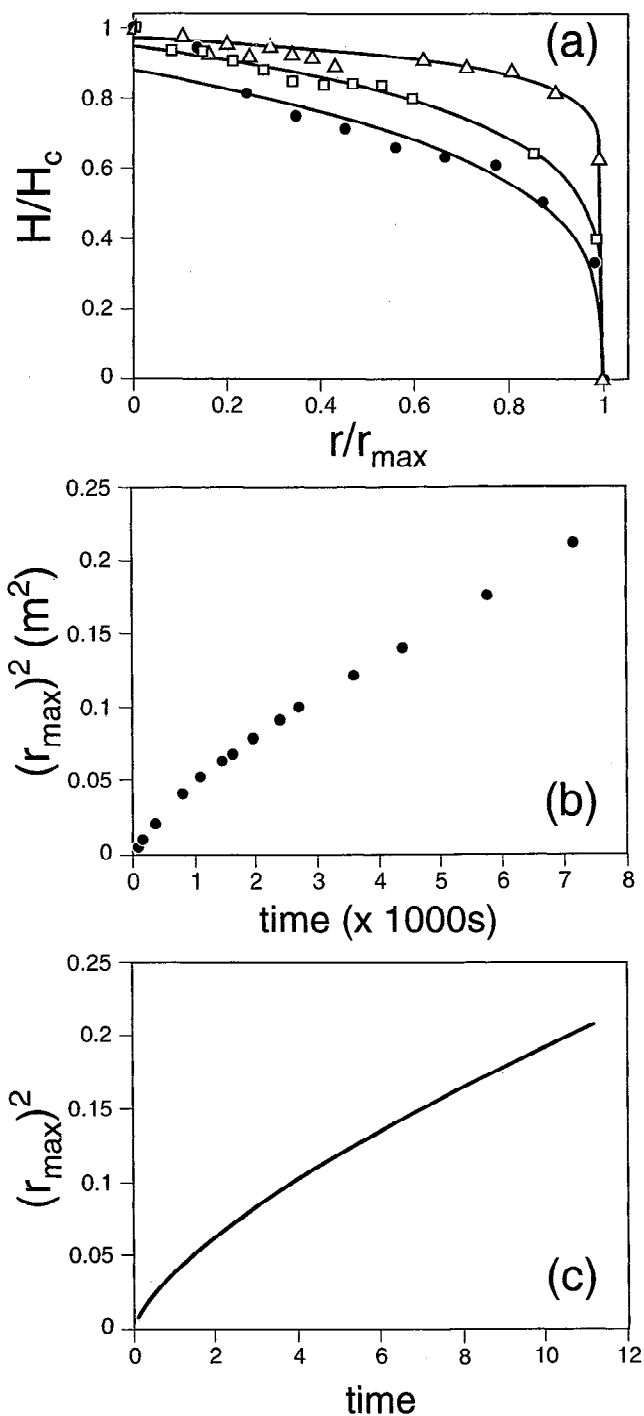
Figure 7. Data for laboratory models of steadily fed cooling viscous gravity currents, after *Stasiuk et al.* [1993]; data are from their experiment 270391. (a) Normalized flow thickness H/H_c versus normalized radius from the feeder conduit r/r_{max} at 600 s (solid circles), 2000 s (squares), and 6000 s (triangles) after the start of the experiment; H_c is the center thickness and is 3.4 cm, 3.9 cm, and 4.6 cm at each consecutive time; r_{max} is the edge radius, which is 18.8 cm, 31.0 cm, and 43.0 cm at each time. (b) Edge radius squared r_{max}^2 versus time for the same experiment. (c) For comparison, dimensionless r_{max}^2 versus t for the constant-flux model gravity current for $\nu = 1000$, $f = 1$ (i.e., the same data as shown in Figure 5). See text and *Stasiuk et al.* [1993] for details on the laboratory experiments.

flow front is largely absent (and is thus not sufficient to cause a significant swell or geoid anomaly), the chemical buoyancy in the flow front may provide significant uplift. (Note that the chemical anomaly in the gravity current model is at all times bounded by the surface $H(r,t)$.) This effect may also provide an alternative explanation for the raised rims and depressed interiors of many Venus coronae [*Squyres et al.*, 1992], assuming they are generated by mantle diapirs.

The most compelling evidence for the frontal swelling effect in the gravity current models of mantle plume heads may be in the petrology and geochemistry of some terrestrial hotspots. Both the Marquesas and Galápagos hotspots have zones enriched in oceanic-island basalts (OIB), which represent plume material, surrounding a central region enriched in mid-ocean ridge basalts (MORB), which represent ambient upper mantle. The OIB-rich zone in the Marquesas is more or less ring shaped [*Duncan et al.*, 1986; *Woodhead*, 1992], while the Galápagos OIB zone displays a horseshoe pattern [*Geist et al.*, 1988; *White et al.*, 1993]. These patterns have been attributed to diapiric plume heads, which become torus shaped as they traverse the deep mantle and entrain upper mantle material [*Griffiths*, 1986], or to steady plumes which develop dual-conduit structures after entraining background mantle [*Richards and Griffiths*, 1989]. However, recent analysis of the geochemical evolution of the Marquesas [*Woodhead*, 1992] discounts entrainment effects of plumes in the deep mantle and favors lithospheric control of magmatic evolution. The applicability of the entrainment mechanism to Galápagos has also been challenged by *Feighner and Richards* [1994], who contend that lithospheric flexure and thinning provide the dominant control of the geochemical signature of Galápagos.

The gravity current model proposed here suggests an alternative mechanism in which the plume head (especially one fed by a steady conduit) may acquire a pseudo-torus shape after it reaches the lithosphere and begins to spread and cool. In particular, the frontal swelling effect induced by temperature-dependent buoyancy leads to the plume chemical anomaly being most concentrated in a ring at the edge of the plume head. The thinner center of the plume head would be relatively depleted in the plume chemical anomaly. Thus the gravity current model, like the entrainment models, can explain how the Marquesas and Galápagos hotspots could have zones of OIB (plume) enriched material surrounding MORB (ambient mantle) enriched centers.

The gravity current and entrainment models, however, differ in one significant prediction. Entrainment models [*Griffiths*, 1986; *Richards and Griffiths*, 1989] indicate that the majority of the plume material is swept into the torus or dual-conduit structure, and thus the plume's thermal anomaly would also reside primarily in the torus or dual conduits. This suggests that the regions of maximum melting would correlate with the OIB-rich zone. The gravity current model, however,

indicates that while the chemical anomaly is concentrated in a ring at the edge of the plume head, the thermal anomaly remains at the center of the plume head (Figure 4, second and fourth frames). This model therefore predicts that the region of maximum melting should coincide with the MORB-rich center of the hotspot. In fact, for both the Marquesas and Galápagos hotspots the greatest volumes of melting and volcanic shield building occur within the MORB-rich regions, while the OIB-rich zones have small melt volumes [*Duncan et al.*, 1986; *Woodhead*, 1992; *White et al.*, 1993]. Thus, the combined petrological and geochemical data appear to lend greater support to the gravity current model than to the entrainment models.

Conclusions

In this paper we have presented a theory for cooling gravity currents which allows for temperature-dependent viscosity and buoyancy. Variations in viscosity are particularly important for many geological fluid mechanics problems involving either the liquid or subsolidus flow of silicates. Thermal variations in density are important for buoyant mantle plume heads spreading beneath the the Earth's lithosphere. The most salient features of our cooling gravity current model are as follows:

1. Before cooling is significant, the gravity currents spread with rates comparable to isothermal gravity currents. Once cooling ensues, the spreading rate slows considerably. This effect causes constant volume currents to collapse more slowly and constant volume flux currents to grow as much by thickening as by spreading, in contrast to the isothermal constant flux currents, which grow exclusively by spreading [*Huppert*, 1982].

2. Gravity currents that have only temperature-dependent viscosity develop steep-sided flat-topped morphologies regardless of whether they are constant volume or constant volume flux. These model currents agree reasonably well with laboratory experiments [*Stasiuk et al.*, 1993], except that they tend to overestimate cooling in the early stages of the current's evolution.

3. Gravity currents that have temperature-dependent buoyancy (with or without variable viscosity) develop inflexions, ridges, and/or swelling at their edges. This result suggests an alternative mechanism for the morphology of the Hawaiian swell. More important, this result provides an explanation for the ring- or horseshoe-shaped geochemical pattern at the Marquesas and Galápagos hotspots that, in contrast to traditional entrainment models, also accounts for the thermal melting pattern.

Appendix A: On the Self-Consistency of a Parabolic Temperature Profile

We wish to examine the physical plausibility of our assumed parabolic temperature profile (3)). Structure in the temperature profile that is more fine scaled than

a parabola may be important. This is particulary true if the gravity current is initially isothermal; i.e., such a gravity current will develop extremely thin thermal boundary layers when it comes into contact with the colder boundaries. However, because these thin boundary layers have large thermal gradients, they conduct heat out of the gravity current rapidly and thus they thicken relatively quickly. It should be noted, however, that the initially isothermal mantle-plume head is a worst-case scenario; plume heads will generally have been in thermal contact with the surrounding mantle for millions of years before reaching the base of the lithosphere and will thus not have perfect isothermal profiles (unless internal mixing is very rapid [cf. *Griffiths and Campbell*, 1990]). Nonetheless, the validity of the parabolic profile is best tested by considering the worst case. Thus, if the fluid in the channel starts nearly isothermally except for extremely thin boundary layers near the top and bottom of the channel, then at issue is how quickly these boundary layers fill the fluid channel to yield an approximately parabolic profile. This problem can be addressed in two stages. First, we consider an unmoving thin layer of matter that is initially at a uniform temperature and subjected to colder boundaries. We then determine how quickly the boundary layers in a portion of the medium thicken in relation to how quickly all the heat from that portion is lost. Second, we look at the effect of the boundary layers being embedded in fluid layers which move sluggishly because they are adjacent to a no-slip boundary and/or have high viscosity.

First, we determine the decay rate for the small-scale structure of the temperature profile (which causes the narrow boundary layers) relative to the decay rate for the bulk temperature anomaly for the solid medium. This can be demonstrated by the simple one-dimensional diffusion of a step function. Consider temperature $T(z,t)$ subject to 1-D diffusion

$$\frac{\partial T}{\partial t} = \kappa \frac{\partial^2 T}{\partial z^2}. \tag{A1}$$

Given boundary conditions $T = 0$ at $z = 0, H$, we can represent T as a sine series (which automatically satisfies the boundary conditions)

$$T = \sum_{n=0}^{\infty} T_n(t) \sin(n\pi z/H) \tag{A2}$$

At $t = 0$ we can assume T is a top hat function, i.e., $T = 1$ for $0 \le z \le H$ and $T = 0$ elsewhere; this assumption leads to

$$T_n(0) = \frac{4}{n\pi} \begin{cases} 1 & n \text{ odd} \\ 0 & n \text{ even} \end{cases}. \tag{A3}$$

Note that even for this top hat function the $n = 1$ mode, which is the half-sine or parabolic mode (these are nearly identical in basic shape), is still the dominant term with 3 times the magnitude of the next largest nonzero mode. Given the 1-D diffusion equation, the

solution for $T_n(t)$ is thus

$$T_n = T_n(0)e^{-\kappa\left(\frac{n\pi}{H}\right)^2 t}. \qquad (A4)$$

Thus all the nonzero terms with $n > 1$ (i.e., only for $n = 3, 5, 7, ...$) which yield the thin boundary layers have exponential decay rates which go as n^2, i.e., at least an order or magnitude faster than the parabolic ($n = 1$) mode. The decay time for each term is thus really $H^2/(n\pi)^2\kappa$. The diffusion time H^2/κ gives the basic timescale for the bulk loss of heat for the entire medium; it is an order of magnitude longer than the parabolic ($n = 1$) mode (because of the π^{-2} factor) and at least 2 orders of magnitude larger than the decay time for the higher-order modes which make the boundary layers narrow. The decay of the thin boundary layer structure thus decays at least 100 times faster than the bulk loss of heat and at least 10 times faster than the dominant parabolic structure.

Not only do the boundary layers grow fast in relation to the overall loss of heat of the medium, they probably do not move a significant distance while growing, especially when the fluid in which the boundary layers are embedded move slowly. This process occurs for fluid adjacent to a no-slip boundary and/or for temperature-dependent viscosity fluid near a cold boundary. In such cases the boundary layers will grow to their maximum thickness over a short distance, and thus the boundary layers are fully adjusted to a parabolic-type profile for most of the length of the gravity current. We demonstrate this effect by considering a simple flat channel (bounded between $z = 0$ and $-H$) driven by an applied pressure gradient; as we are only interested in the growth of the thermal boundary layers (and whether their structure is consistent with the assumed parabolic profile), we do not concern ourselves with the deformability of the channel. For simplicity and symmetry we consider both channel walls to be no-slip and the applied radial pressure gradient to be independent of z. We then test the appropriateness of our assumed parabolic temperature profile as a solution to a boundary layer temperature equation. First, we integrate (1) to obtain v_r as a function of temperature:

$$v_r = \frac{1}{2\mu_h\mu_c}\frac{\partial P}{\partial r}z(H + z)\left[\mu_h - 3\Delta\mu\Theta\frac{z}{H}\left(1 + \frac{z}{H}\right)\right] \qquad (A5)$$

which can be rewritten (by using (3)) as

$$v_r = \frac{H^2}{2\mu_c}\frac{\partial P}{\partial r}\frac{z}{H}\left(1 + \frac{z}{H}\right)\left[1 + \frac{\Delta\mu}{2\mu_h}\theta\right] \qquad (A6)$$

where $\Delta\mu = \mu_c - \mu_h$. We employ this v_r in the steady boundary layer equation

$$v_r\frac{\partial\theta}{\partial r} = \kappa\frac{\partial^2\theta}{\partial z^2} \qquad (A7)$$

to solve for the basic form of θ and estimate how the

boundary layers grow with horizontal distance. For steady flow we assume H is constant. We prescribe a general pressure gradient independent of z:

$$\frac{\partial P}{\partial r} = -\frac{P_o}{R}\phi(r) \qquad (A8)$$

where P_o is a pressure scale, $R = H^2(P_o/2\mu_c\kappa)^{1/2}$, and ϕ is some arbitrary function of r. Thus, by nondimensionalizing z by H and r by R, the steady boundary layer equation becomes

$$-\phi(r)z(1 + z)\left(1 + \frac{\nu'}{2}\theta\right)\frac{\partial\theta}{\partial r} = \frac{\partial^2\theta}{\partial z^2} \qquad (A9)$$

where $\nu' = \Delta\mu/\mu_h$. If we define $A = 1 + \nu'\Theta/2$, then the boundary layer equation becomes

$$-\phi(r)z(1 + z)A\frac{\partial A}{\partial r} = \frac{\partial^2 A}{\partial z^2}. \qquad (A10)$$

Assuming $A = \beta(r)\psi(z)$ (i.e., that A is separable), this equation becomes

$$\phi(r)\frac{d\beta}{dr} = \frac{-1}{z(1 + z)\psi^2}\frac{d^2\psi}{dz^2} = -\alpha^2 \qquad (A11)$$

where α^2 is necessarily a constant eigenvalue. Equation (A11) leads to $\beta = \beta_o - \alpha^2\int dr/\phi(r)$ (where β_o is a constant) and

$$\frac{d^2\psi}{dz^2} - \alpha^2 z(1 + z)\psi^2 = 0. \qquad (A12)$$

We are primarily concerned with the form of ψ (since we wish to test the self-consistency of the vertical parabolic temperature profile). We choose the boundary conditions $\psi = \psi_o$ (a constant) at $z = 0, -1$ and solve (A12) numerically. (The numerical solution of the eigenvalue α^2 demands an additional constraint: Assuming that $\psi(z)$ is symmetric about $z = -1/2$, we require that $\psi'(0) = -\psi'(-1)$.) Figure A1 shows a numerical solution for ψ with $\psi_o = 1$. Different choices of ψ_o and initial guesses in α^2 and the boundary values of ψ' simply change the amplitude of ψ and the final value of α^2, but always yield the same-shaped profile. It is apparent that the parabolic profile is a good approximation to $\psi(z)$ and hence is at least a self-consistent approximation to the vertical temperature profile, even near the inlet to the channel. This result implies that the thermal boundary layers thicken over a very short distance. As was suggested by our comparison to the laboratory experiments of *Stasiuk et al.* [1993], these boundary layers do indeed adjust over a distance considerably shorter than the length of the flow, but they undoubtedly do not adjust within an infinitesimal distance, as our theory assumes.

Finally, we note that although this paper is concerned with the problem of cooling gravity currents, heated gravity currents (as applicable to cold descending slab
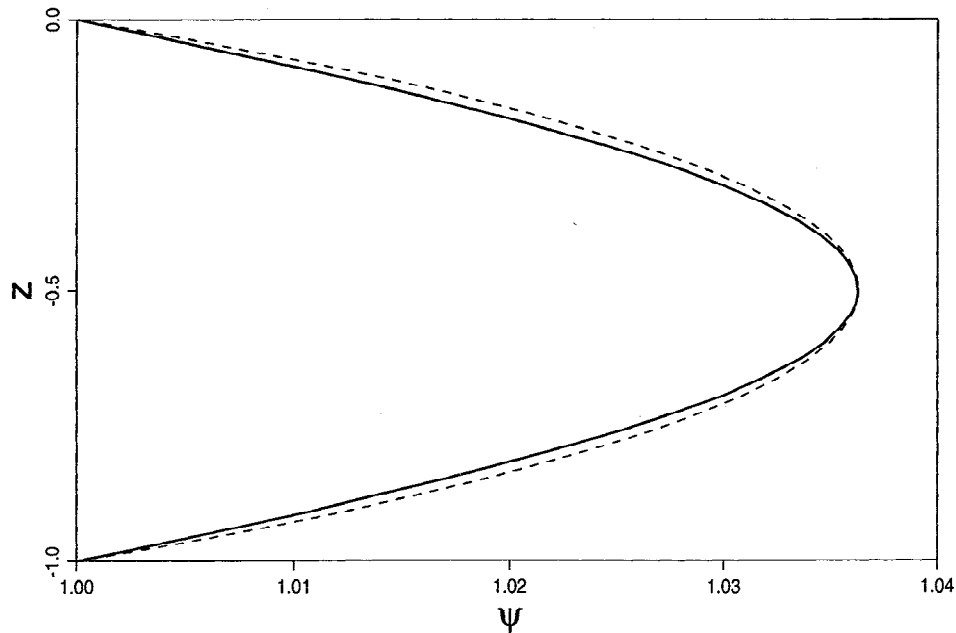
Figure A1. Numerical solution of (A12) (solid line) (see Appendix A) and a parabola with the same minimum and maximum values (dashed line). The boundary values of ψ are $\psi_o = 1$ and initial guesses for $\psi'(-1)$ and α^2 were 1. The numerical solution yields a final eigenvalue of $\alpha^2 = 1.3115$.

material pooling on a heated interface [see *Kerr and Lister*, 1987; *Bercovici et al.*, 1993; *Koch and Koch*, 1995]) can be obtained by following the theory presented here and replacing (3) with

$$\theta(r, z, t) = 3\Theta(r, t) \left[1 + 4\frac{z}{H} \left(1 + \frac{z}{H} \right) \right] \qquad (A13)$$

such that θ would be 0 at the center of the current and 3Θ at current's top and bottom.

Appendix B: Radial Velocity, Volumetric Flux, and Thermal Flux

We here consider the derivation of the radial velocity v_r and and flux (per unit length in the azimuthal direction) q. Two integrations of (1) over height z lead to the (dimensional) radial velocity,

$$\begin{aligned}
v_r &= \frac{\Delta\rho_C g}{\mu_h \mu_c} \frac{\partial H}{\partial r} M_1(z) + \frac{\Delta\rho_T g}{\mu_h \mu_c} \left[\left(M_1(z) + \frac{M_3(z)}{H^2} \right. \right. \\
&\quad \left. + \frac{M_4(z)}{H^3} \right) \Theta \frac{\partial H}{\partial r} + \left(M_1(z) - \frac{M_3(z)}{H^2} \right. \\
&\quad \left. \left. - \frac{M_4(z)}{2H^3} \right) H \frac{\partial\Theta}{\partial r} \right] + K M_0(z) \qquad (B1)
\end{aligned}$$

in which

$$\begin{aligned}
M_n(z) &= \int \left[\mu_h - 6\Delta\mu\Theta\frac{z}{H} \left(1 + \frac{z}{H} \right) \right] z^n dz \\
&= \frac{\mu_h z^{n+1}}{n+1} - 6\Delta\mu\Theta \left(\frac{z^{n+2}}{(n+2)H} \right.
\end{aligned}$$

$$\left. + \frac{z^{n+3}}{(n+3)H^2} \right) \qquad (B2)$$

where $\Delta\mu = \mu_c - \mu_h$. The integration constant K is

$$K = \frac{\Delta\rho_C g H}{\mu_h \mu_c} \frac{\partial H}{\partial r} + \frac{\Delta\rho_T g H}{\mu_h \mu_c} \left[\Theta\frac{\partial H}{\partial r} + \frac{H}{2} \frac{\partial\Theta}{\partial r} \right] \qquad (B3)$$

if the boundary at $z = -H$ is free-slip (i.e., $\partial v_r/\partial z = 0$) and

$$\begin{aligned}
K &= \frac{\Delta\rho_C g H}{2\mu_h \mu_c} \frac{\partial H}{\partial r} + \frac{\Delta\rho_T g H}{2\mu_h \mu_c} \left[\left(1 + \frac{\mu_h + \frac{4}{5}\Delta\mu\Theta}{2(\mu_h + \Delta\mu\Theta)} \right. \right. \\
&\quad \left. - \frac{2(\mu_h + \frac{5}{7}\Delta\mu\Theta)}{5(\mu_h + \Delta\mu\Theta)} \right) \Theta\frac{\partial H}{\partial r} + \left(1 - \frac{\mu_h + \frac{4}{5}\Delta\mu\Theta}{2(\mu_h + \Delta\mu\Theta)} \right. \\
&\quad \left. \left. + \frac{\mu_h + \frac{5}{7}\Delta\mu\Theta}{5(\mu_h + \Delta\mu\Theta)} \right) H\frac{\partial\Theta}{\partial r} \right] \qquad (B4)
\end{aligned}$$

if the boundary at $z = -H$ is no-slip (i.e., $v_r = 0$). Integrating v_r over the thickness of the layer, we obtain

$$\begin{aligned}
q &= \int_{-H}^{0} v_r dz = \frac{\Delta\rho_C g}{\mu_h \mu_c} \frac{\partial H}{\partial r} F_1 \\
&\quad + \frac{\Delta\rho_T g}{\mu_h \mu_c} \left[\left(F_1 + \frac{F_3}{H^2} + \frac{F_4}{H^3} \right) \Theta\frac{\partial H}{\partial r} \right. \\
&\quad \left. + \left(F_1 - \frac{F_3}{H^2} - \frac{F_4}{2H^3} \right) H\frac{\partial\Theta}{\partial r} \right] + K F_0 \qquad (B5)
\end{aligned}$$

where

$$F_n = \int_{-H}^0 M_n(z)dz = \frac{(-1)^{n+3}H^{n+2}}{n+2}$$
$$\times \left[\frac{\mu_h}{n+1} + \frac{12\Delta\mu\Theta}{(n+3)(n+4)}\right]. \quad (B6)$$

Thus, we obtain

$$q = -\frac{\Delta\rho g H^3}{3\mu_h\mu_c}(\mu_h + \frac{9}{10}\Delta\mu\Theta)\left[f\frac{\partial H}{\partial r}\right.$$
$$+\frac{7}{20}(1-f)\left(\frac{\mu_h + \frac{75}{98}\Delta\mu\Theta}{\mu_h + \frac{9}{10}\Delta\mu\Theta}\right)\frac{\partial(\Theta H)}{\partial r}$$
$$\left.+\frac{3}{5}(1-f)\left(\frac{\mu_h + \frac{53}{56}\Delta\mu\Theta}{\mu_h + \frac{9}{10}\Delta\mu\Theta}\right)\Theta\frac{\partial H}{\partial r}\right] \quad (B7)$$

(where $\Delta\rho = \Delta\rho_C + \Delta\rho_T$ and $f = \Delta\rho_C/\Delta\rho$) if the boundary at $z = -H$ is free-slip and

$$q = -\frac{\Delta\rho g H^3}{12\mu_h\mu_c}(\mu_h + \frac{3}{5}\Delta\mu\Theta)\left[f\frac{\partial H}{\partial r}\right.$$
$$+\frac{1}{2}(1-f)\frac{\partial(\Theta H)}{\partial r}$$
$$\left.+\frac{3}{5}(1-f)\left(\frac{\mu_h + \frac{9}{14}\Delta\mu\Theta}{\mu_h + \frac{3}{5}\Delta\mu\Theta}\right)\Theta\frac{\partial H}{\partial r}\right] \quad (B8)$$

if the boundary at $z = -H$ is no-slip. The ratios

$$\frac{\mu_h + \frac{75}{98}\Delta\mu\Theta}{\mu_h + \frac{9}{10}\Delta\mu\Theta}, \quad \frac{\mu_h + \frac{53}{56}\Delta\mu\Theta}{\mu_h + \frac{9}{10}\Delta\mu\Theta}, \quad \frac{\mu_h + \frac{9}{14}\Delta\mu\Theta}{\mu_h + \frac{3}{5}\Delta\mu\Theta} \quad (B9)$$

are all $O(1)$ regardless of Θ and are hence set to unity for the sake of simplicity. This assumption leads to

$$q = -\frac{\Delta\rho g H^3}{3\mu_h\mu_c}(\mu_h + \frac{9}{10}\Delta\mu\Theta)\left[f\frac{\partial H}{\partial r}\right.$$
$$\left.+(1-f)\left(\frac{7}{20}H\frac{\partial\Theta}{\partial r} + \frac{19}{20}\Theta\frac{\partial H}{\partial r}\right)\right] \quad (B10)$$

if the lower boundary is free-slip and

$$q = -\frac{\Delta\rho g H^3}{12\mu_h\mu_c}(\mu_h + \frac{3}{5}\Delta\mu\Theta)\left[f\frac{\partial H}{\partial r}\right.$$
$$\left.+(1-f)\left(\frac{1}{2}H\frac{\partial\Theta}{\partial r} + \frac{11}{10}\Theta\frac{\partial H}{\partial r}\right)\right] \quad (B11)$$

if the lower boundary is no-slip. Given the approximate nature of the overall theory, 7/20 does not differ enough from 1/2, nor do 19/20 and 11/10 differ enough from unity, to warrant using different formulae for q with each boundary condition. Thus we approximate 7/20 with 1/2 (given that 7 is $O(10)$) and replace both 19/20 and 11/10 with 1 to obtain (after some slight rearrangement) (6), with (7) or (8).

Table B1. Comparison of the Coefficients G_n and F_n to Test the Accuracy of the Approximation $\int_{-H}^0 \theta v_r\, dz \approx \Theta q$

n	F_n/H^{n+2}	G_n/H^{n+2}
0	$-\frac{1}{2}(\mu_h + \Delta\mu\Theta)$	$-\frac{1}{2}(\mu_h + \Delta\mu\Theta)$
1	$\frac{1}{6}(\mu_h + \frac{6}{5}\Delta\mu\Theta)$	$\frac{3}{20}(\mu_h + \frac{26}{21}\Delta\mu\Theta)$
3	$\frac{1}{20}(\mu_h + \frac{8}{7}\Delta\mu\Theta)$	$\frac{1}{28}(\mu_h + \frac{13}{15}\Delta\mu\Theta)$
4	$-\frac{1}{30}(\mu_h + \frac{15}{14}\Delta\mu\Theta)$	$-\frac{3}{140}(\mu_h + \frac{11}{9}\Delta\mu\Theta)$

Only those values of n that are employed in the theory are shown. See Table 1 and Appendix B for definition of symbols.

We finally wish to examine the accuracy of the relation

$$\int_{-H}^0 \theta v_r dz \approx \Theta q \quad (B12)$$

which is necessary to derive the one-dimensional temperature equation, in particular to go from (13) to (14). Using (3) and (B1), we obtain

$$\int_{-H}^0 \theta v_r dz = \Theta\left(\frac{\Delta\rho_C g}{\mu_h\mu_c}\frac{\partial H}{\partial r}G_1 + \frac{\Delta\rho_T g}{\mu_h\mu_c}\left[\left(G_1\right.\right.\right.$$
$$\left.+\frac{G_3}{H^2} + \frac{G_4}{H^3}\right)\Theta\frac{\partial H}{\partial r} + \left(G_1 - \frac{G_3}{H^2}\right.$$
$$\left.\left.\left.-\frac{G_4}{2H^3}\right)H\frac{\partial\Theta}{\partial r}\right] + KG_0\right) \quad (B13)$$

where

$$G_n = -6\int_{-H}^0 M_n(z)\frac{z}{H}\left(1 + \frac{z}{H}\right)dz$$
$$= 6(-1)^{n+3}H^{n+2}\left(\frac{\mu_h}{(n+1)(n+3)(n+4)}\right.$$
$$+6\Delta\mu\Theta\left[\frac{1}{(n+2)(n+4)} + \frac{1}{(n+3)(n+6)}\right.$$
$$\left.\left.-\frac{2n+5}{(n+2)(n+3)(n+5)}\right]\right). \quad (B14)$$

Thus the accuracy of (B12) depends on whether $G_n \approx F_n$ (see (B5) and (B6)); this approximation is in general quite accurate, as shown in Table B1.

References

Bercovici, D., Wave dynamics in mantle plume heads and hotspot swells, Geophys. Res. Lett., 19, 1791–1794, 1992.

Bercovici, D., A theoretical model of cooling viscous gravity currents with temperature-dependent viscosity, *Geophys. Res. Lett. 21*, 1177–1180, 1994.

Bercovici, D., G. Schubert, and P. J. Tackley, On the penetration of the 660-km phase change by mantle downflows, *Geophys. Res. Lett., 20*, 2599–2602, 1993.

Crisp, J., and S. Baloga, A model for lava flow with two thermal components, *J. Geophys. Res., 95*, 1255–1270, 1990.

Didden, N., and T. Maxworthy, The viscous spreading of plane and axisymmetric gravity currents, *J. Fluid Mech., 121*, 27–42, 1982.

Duncan, R. A., M. T. McCulloch, H. G. Barsczus, and D. R. Nelson, Plume versus lithospheric sources for melts at Ua Pou, Marquesas Islands, *Nature, 322*, 534–538, 1986.

Feighner, M. A., and M. A. Richards, Lithospheric structure and compensation mechanisms of the Galápagos Archipelago, *J. Geophys. Res., 99*, 6711–6729, 1994.

Fink, J. H., and R. W. Griffiths, Radial spreading of viscous-gravity currents with solidifying crust, *J. Fluid Mech., 221*, 485–509, 1990.

Fink, J. H., and R. W. Griffiths, A laboratory analog study of the surface morphology of lava flows extruded from point and line sources, *J. Volcanol. Geotherm. Res, 54*, 19–32, 1992.

Geist, D. J., W. M. White, and A. R. McBirney, Plume-asthenosphere mixing beneath the Galápagos Archipelago, *Nature, 333*, 657–660, 1988.

Griffiths, R. W., The differing effects of compositional and thermal buoyancies on the evolution of mantle diapirs, *Phys. Earth. Planet. Inter., 43*, 261–273, 1986.

Griffiths, R. W., and I. H. Campbell, Stirring and structure in mantle starting plumes, *Earth Planet. Sci. Lett., 99*, 66–78, 1990.

Griffiths, R. W., and I. H. Campbell, On the dynamics of long-lived plume conduits in the convecting mantle, *Earth Planet. Sci. Lett., 103*, 214–227, 1991a.

Griffiths, R. W., and I. H. Campbell, Interaction of mantle plume heads with the Earth's surface and onset of small-scale convection, *J. Geophys. Res., 96*, 18,295–18,310, 1991b.

Griffiths, R. W., and J. H. Fink, Effects of surface cooling on the spreading of lava flows and domes, *J. Fluid Mech., 252*, 667–702, 1993.

Griffiths, R. W., M. Gurnis, and G. Eitelberg, Holographic measurements of surface topography in laboratory models of mantle hotspots, *Geophys. J., 96*, 477–495, 1989.

Helfrich, K. R., and J. A. Whitehead, Solitary waves on conduits of buoyant fluid in a more viscous fluid, *Geophys. Astrophys. Fluid Dyn., 51*, 35–52, 1990.

Huppert, H. E., The propagation of two-dimensional and ax-isymmetric viscous gravity currents over a rigid horizontal surface, *J. Fluid. Mech., 121*, 43–58, 1982

Huppert, H. E., J. B. Shepherd, H. Sigurdsson, and R. S. J. Sparks, On lava dome growth, with application to the 1979 lava extrusion of the Soufrière of St. Vincent, *J. Volcanol. Geotherm. Res, 14*, 199–222, 1982.

Kerr, R. C., and J. R. Lister, The spread of subducted lithospheric material along the mid-mantle boundary, *Earth Planet. Sci., 85*, 241–247, 1987.

Koch, D. M., and D. L. Koch, Numerical and theoretical solutions for a drop spreading below a free fluid surface, *J. Fluid Mech., 287*, 251–278, 1995.

Lister, J. R., and R. C. Kerr, The propagation of two-dimensional and axisymmetric viscous gravity currents at a fluid interface, *J. Fluid Mech., 203*, 215–249, 1989.

Loper, D. E., and F. D. Stacey, The dynamical and thermal structure of deep mantle plumes, *Phys. Earth Planet. Inter., 33*, 304–317, 1983.

McNutt, M. K., and L. Shure, Estimating the compensation depth of the Hawaiian swell with linear filters, *J. Geophys. Res., 91*, 13,915–13,924, 1986.

Olson, P., Hot spots, swells and mantle plumes, in *Magma Transport and Storage*, edited by M.P. Ryan, pp.33–51, John Wiley, New York, 1990.

Olson, P., Mechanics of flood basalt magmatism, in *Magmatic Systems*, edited by M.P. Ryan, pp. 1–18, Academic, San Diego, Calif., 1994.

Olson, P., and U. Christensen, Solitary wave propagation in a fluid conduit within a viscous matrix, *J. Geophys. Res., 91*, 6367–6374, 1986.

Olson, P., and I. S. Nam, The formation of sea floor swell by mantle plumes, *J. Geophys. Res., 91*, 7181–7191, 1986.

Olson, P., and H. Singer, Creeping plumes, *J. Fluid Mech., 158*, 511–531, 1985.

Pavri, B., J. W. Head, K. B. Klose, and L. Wilson, Steep-sided domes on Venus: Characteristics, geologic setting, and eruption conditions from Magellan data, *J. Geophys. Res., 97*, 13,445–13,478, 1992.

Patankar, S. V., *Numerical Heat Transfer and Fluid Flow*, Taylor and Francis, Bristol, Pa., 1980.

Phipps Morgan, J., W. J. Morgan, and E. Price, Hotspot melting generates both hotspot volcanism and a hotspot swell?, *J. Geophys. Res., 100*, 8045–8062, 1995.

Ribe, N. M., and U. R. Christensen, Three-dimensional modeling of plume-lithosphere interaction, *J. Geophys. Res., 99*, 669–682, 1994.

Richards, M. A., and R. W. Griffiths, Thermal entrainment by deflected mantle plumes, *Nature, 342*, 900–902, 1989.

Sakimoto, S. E. H., and M. T. Zuber, The spreading of variable viscosity axisymmetric radial gravity currents: Applications to the emplacement of Venus "pancake" domes, *J. Fluid Mech., 301*, 65–77, 1995.

Schubert, G., P. Olson, C. Anderson, and P. Goldman, Solitary waves in mantle plumes, *J. Geophys. Res., 94*, 9523–9532, 1989.

Scott, D. R., D. J. Stevenson, and J. A. Whitehead, Observations of solitary waves in a viscously deformable pipe, *Nature, 319*, 759–761, 1986.

Skilbeck, J. N., and J. A. Whitehead, Formation of discrete islands in linear island chains, *Nature, 272*, 499–501, 1978.

Sleep, N. H., Hotspots and mantle plumes: Some phenomenology, *J. Geophys. Res., 95*, 6715–6736, 1990.

Smith, D. K. and J. R. Cann, Building the crust at the Mid-Atlantic Ridge, *Nature, 365*, 707–715, 1993.

Smith, D. K., et al., Mid-Atlantic Ridge volcanism from deep-towed side-scan sonar images, 25°-29°N, *J. Volcanol. Geotherm. Res., 67*, 233–262, 1995.

Squyres, S. W., D. M. Janes, G. Baer, D. L. Bindschadler, G. Schubert, V. L. Scharpton, and E. R. Stofan, The morphology and evolution of coronae on Venus, *J. Geophys. Res., 97*, 13,611–13,634, 1992.

Stasiuk, M. V., C. Jaupart, and R. S. J. Sparks, Influence of cooling on lava-flow dynamics, *Geology, 21*, 335–338, 1993.

ten Brink, U. S., Volcano spacing and plate rigidity, *Geology, 19*, 397–400, 1991.

Vogt, P. R., Volcano spacing, fractures, and thickness of the lithosphere, *Earth Planet. Sci. Lett., 21*, 235–252, 1974.

Wessel, P., Observational constraints on models of the Hawaiian hot spot swell, *J. Geophys. Res., 98*, 16,095–16,104, 1993.

White, W. M., A. R. McBirney, and R. A. Duncan, Petrology and geochemistry of the Galápagos Islands: Portrait of a pathological mantle plume, *J. Geophys. Res., 98*, 19,533–19,563, 1993.

Woodhead, J. D., Temporal geochemical evolution in oceanic intra-plate volcanics: A case study from the Marquesas (French Polynesia) and comparison to other hotspots, *Contrib. Mineral. Petrol., 111*, 458–467, 1992.

D. Bercovici, Department of Geology and Geophysics, School of Ocean and Earth Science and Technology, University of Hawaii, 2525 Correa Road, Honolulu, HI 96822 (e-mail: dberco@soest.hawaii.edu)

J. Lin, Department of Geology and Geophysics, Woods Hole Oceanographic Institution, Woods Hole, MA 02543 (e-mail: jian@galileo.whoi.edu)